Journal of Computational and Applied Mathematics 236 (2012) 4933–4943

Contents lists available at SciVerse ScienceDirect

Journal of Computational and Applied Mathematics

journal homepage: www.elsevier.com/locate/cam

Non-isothermal, compressible gas flow for the simulation of an enhanced gas recovery application

N. Böttcher [a,*], A.-K. Singh [b], O. Kolditz [b,c], R. Liedl [a]

[a] Technische Universität Dresden, Institute for Groundwater Management, 01062 Dresden, Germany

[b] Department of Environmental Informatics, Helmholtz-Centre for Environmental Research - UFZ, Permoserstr. 15, 04318 Leipzig, Germany

[c] Technische Universität Dresden, Applied Environmental Systems Analysis, 01062 Dresden, Germany

ARTICLE INFO

Article history:
Received 29 July 2011
Received in revised form 15 November 2011

Keywords:
Carbon dioxide sequestration
Enhanced gas recovery
Numerical simulation
Real gas behavior
Equation of state
Finite element method

ABSTRACT

In this work, we present a framework for numerical modeling of CO_2 injection into porous media for enhanced gas recovery (EGR) from depleted reservoirs. Physically, we have to deal with non-isothermal, compressible gas flows resulting in a system of coupled non-linear PDEs. We describe the mathematical framework for the underlying balance equations as well as the equations of state for mixing gases. We use an object-oriented finite element method implemented in C++. The numerical model has been tested against an analytical solution for a simplified problem and then applied to CO_2 injection into a real reservoir. Numerical modeling allows to investigate physical phenomena and to predict reservoir pressures as well as temperatures depending on injection scenarios and is therefore a useful tool for applied numerical analysis.

1. Introduction

The rate of anthropogenic CO_2-emissions into the atmosphere has been increasing since the era of industrialization in the early twentieth century. Most likely, this raise will continue in the future, since the growth of earth population and the technological progress will increase energy demands [1]. On the other hand, there are few emission-free energy sources available, so energy from fossil fuels is still one of the most important power sources.

To reduce the amount of the green-house gas carbon dioxide in the atmosphere, much research has been done and many strategies in different scientific disciplines have been presented till this day. Carbon dioxide capture and storage (CCS) is one of those concepts to reduce the atmospheric CO_2 emission. Among other methods, such as the injection of CO_2 into saline aquifers (see CO_2-MOPA [2] and CO_2-SINK [3] for related projects), the concept of enhanced gas recovery (EGR) is one of the most promising CCS technologies. The idea of the EGR method is to raise the production of natural gases by injecting purified CO_2 from power plant emissions into depleted gas reservoirs. Fig. 1 depicts a schematic of this concept. By injecting CO_2 in the gas field, the reservoir pressure will be increasing slowly up to its former natural level. This method has several advantages: first, large amounts of CO_2 originating from sub-surface fossil fuels will be stored in the underground again and are not enriching the atmosphere with greenhouse gases. Second, the pressure in a depleted gas reservoir is much lower than in undisturbed natural gas reservoirs. The increase of pressure up to natural levels by injecting CO_2 would reduce the risk of subsidence and landslides. The third advantage is that due to the increased pressure in the reservoir, residing amounts of fossil natural gases such as methane or ethane can be produced from a site, which was considered almost to be depleted when using conventional gas production technologies. In previous works [4–6], the concept of enhanced gas recovery has

* Corresponding author.
E-mail address: norbert.boettcher@tu-dresden.de (N. Böttcher).

0377-0427/$ – see front matter © 2011 Elsevier B.V. All rights reserved.
doi:10.1016/j.cam.2011.11.013

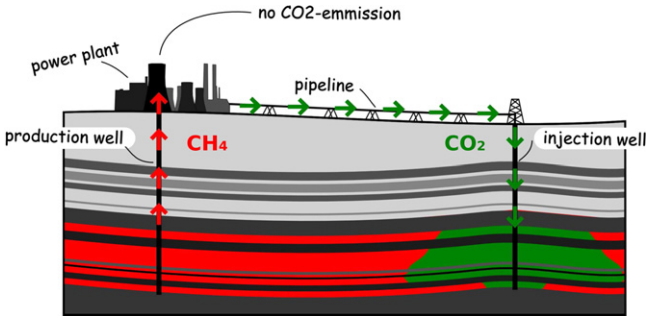

Fig. 1. Schematic of the EGR method.

been investigated in terms of feasibility and has been judged as promising [7]. With the CLEAN project [8], Germany started a large research initiative to investigate the suitability of the EGR method for Europe's second largest onshore gas field [9]. This reservoir is located in the *Altmark* (Germany) and owned by GDF SUEZ E&P Deutschland GmbH. The aim of CLEAN is to find methods and strategies for a safe and economic application of CO_2 sequestration.

The underground storage of CO_2 is a complex process with a high bandwidth of consequences. Among natural leaks such as faults, CO_2 may escape from the storage reservoir through man-made preferential flow paths such as abandoned or leaky wells. Therefore, it is very important that all possible side effects are investigated carefully. Some issues of the storage process side effects, e.g. the long-term integrity of the cap rock, can only be investigated by performing numerical simulations. Various simulations have been performed to appraise the risks of mechanical failure of the rock matrix [10,11] or the chemical reactions occurring in the geological formation [12]. Blok et al. [4] and van der Burgt [6] investigated the mixing processes of CO_2 and natural gas in detail. Due to diffusion, concentration gradients equilibrate over the time. At a certain point, the EGR method is no longer economical.

In this work, we present a numerical simulation tool for non-isothermal, compressible flows and transport of real gases. The numerical methods we present are compared to an analytical solution for a simplified problem. In addition, we design a model of the near-well gas reservoir of the *Altmark* gas field located in northern Germany and perform a simulation of the CO_2 injection process. The simulation tool has been implemented into the open-source simulator OpenGeoSys (OGS). The tool can be used to design EGR strategies and to estimate the feasibility of a possible CCS application.

2. Theory

2.1. Mass balance equation

In this work, we are simulating the storage of carbon dioxide in a natural gas reservoir. Pressure and temperature conditions for such a purpose may spread widely depending largely on the reservoir conditions, CO_2 and natural gas may exist either in gaseous, liquid, or supercritical state. Thus, we must describe the flow of compressible fluids within the porous gas reservoir. Since gases are completely miscible, fluid mechanics is restricted to single phase flow. The movement of fluids in porous media has been described in [13] as

$$\nabla \cdot (\rho \mathbf{v}) + \frac{\partial (\rho n)}{\partial t} = \rho q_0 \tag{1}$$

where ρ is the fluid density, n is the porosity of the medium and q_0 is a volume flux density of sources or sinks and t is time. The *Darcy* flux vector $\mathbf{v}$ is defined by

$$\mathbf{v} = -\frac{k}{\mu} \nabla p \tag{2}$$

where k is material permeability, μ is the dynamic viscosity of the fluid and p is pressure. We are assuming that the porous medium is stiff, so porosity is not changing over time or pressure. Furthermore, we consider the fluid to be compressible, but we neglect density variations due to temperature changes, so $d\rho/dT = 0$. Inserting (2) in (1), we obtain

$$\nabla \cdot \left(\frac{k\rho}{\mu} \nabla p \right) = n \frac{d\rho}{dp} \frac{\partial p}{\partial t} - \rho q_0. \tag{3}$$

Here, the term $d\rho/dp$ specifies the change of fluid density when pressure is changing. This is actually a derivative of the equation of state of the fluid. Since there are several equations of state existing and since most of them are hard to derive, we want to avoid this expression and use the compressibility factor Z instead. This factor describes the deviation of the

fluid behavior from an ideal gas, and it allows us to express fluid compressibility independently from the chosen equation of state. The compressibility factor of a fluid is a function of pressure and temperature and can be defined as

$$Z = \frac{Mp}{R\rho T} \tag{4}$$

with molar mass M and the universal gas constant $R = 8.314472\ \mathrm{J\,mol^{-1}\,K^{-1}}$. To obtain the pressure dependency of density, $d\rho/dp$, we transform (4) to ρ,

$$\rho = \frac{Mp}{ZRT} \tag{5}$$

and derive it with respect to pressure:

$$\frac{d\rho}{dp} = \frac{M}{RT}\left(Z - p\frac{dZ}{dp}\right)\frac{1}{Z^2}. \tag{6}$$

By substituting $\frac{M}{RT} = \frac{Z\rho}{p}$ and transforming we obtain

$$\frac{1}{\rho}\frac{d\rho}{dp} = \frac{1}{p} - \frac{1}{Z}\frac{dZ}{dp} = \beta_f \tag{7}$$

where β_f is the compressibility of the fluid, which is expressed here in terms of compressibility factor Z. This has the advantage, that we can express the fluid's compressibility even without having chosen a suitable equation of state. Inserting (5) and (7) in (1), we obtain a flow equation for compressible fluids in stiff porous media:

$$\nabla\cdot\left(\frac{kp}{\mu Z}\nabla p\right) = \frac{n\beta_f p}{Z}\frac{\partial p}{\partial t} - \frac{p}{Z}q_0. \tag{8}$$

2.2. Mass balance equation for species

We consider a mixture of residing gases (75% nitrogen, 25% methane) to be one single, homogeneous component called *natural gas*. The injected CO_2 is treated as the second component which is transported within the gaseous phase. Component transport within a gas phase can be described by the advection–dispersion equation

$$n\frac{\partial C}{\partial t} + \nabla\cdot(n\mathbf{v}C) - \nabla\cdot(n\nabla D\cdot\nabla C) = q_m \tag{9}$$

where C is the concentration of the component, q_m is the mass flux density of sources and sinks, and $\mathbf{D}$ is the tensor of hydrodynamic dispersion [13] given by

$$\mathbf{D} = \tau D_m\mathbf{I} + \alpha_T|\mathbf{v}|\mathbf{I} + (\alpha_L - \alpha_T)\frac{v_i v_j}{|\mathbf{v}|}. \tag{10}$$

D_m is molecular diffusion coefficient, τ is tortuosity and α is longitudinal or transversal dispersivity, respectively.

2.3. Energy balance equation

In practice, gas injected into a geological formation cannot be heated up to reservoir temperature (even if this is preferable) due to resulting high energy costs. In order to determine non-linear fluid properties (such as density, viscosity, compressibility) at each point of the reservoir, we included the heat transport process into consideration. In general, the injected CO_2 is colder than the reservoir gas, so the formation will be cooled down. The heat transport process within the solid rock skeleton is described by

$$(1-n)\,\rho^s c_p^s\frac{\partial T}{\partial t} + \nabla\cdot\mathbf{u}^s = q_t^s. \tag{11}$$

Unlike the mass transport equation (9), the heat transport process involves the solid rock skeleton of the reservoir. Heat storage, the first term in (11), and heat conduction, the second term, occurs in the solid as well as in the fluid phase. Heat transport in the fluid is given by

$$n\rho^f c_p^f\frac{\partial T}{\partial t} + \rho^f c_p^f n\mathbf{v}\nabla\cdot T + \nabla\cdot\mathbf{u}^f = q_t^f \tag{12}$$

where the second term represents the convective transport of heat. In (11) and (13), the superscripted s and f stand for solid and fluid respectively and c_p is specific heat capacity. Non-isothermal effects, which appear when gases expand, such as

Joule–Thomson effect and viscous heat dissipation are neglected in this case. Those non-linear effects are discussed in more detail in [14]. Assuming local thermal equilibrium, we obtain the heat transport equation of the porous medium by adding (11) and (13),

$$\left(\rho c_p\right)_{\text{eff}} \frac{\partial T}{\partial t} + \rho^f c_p^f n \mathbf{v} \nabla \cdot T + \nabla \cdot \mathbf{u} = q_t^f \tag{13}$$

where $(\rho c_p)_{\text{eff}}$ is the effective heat capacity of the porous medium given by $(\rho c_p)_{\text{eff}} = (1-n)\rho^s c_p^s + n\rho^f c_p^f$ and $\mathbf{u}$ is conductive heat flux given by *Fourier*'s law

$$\mathbf{u} = \mathbf{u}^s + \mathbf{u}^f = -\lambda_{\text{eff}} \nabla T \tag{14}$$

with effective thermal conductivity $\lambda_{\text{eff}} = (1-n)\lambda^s + n\lambda^f$.

2.4. Fluid properties

To compute the real gas behavior of the fluids, we use the cubic equation of state presented in [15]. This equation is easy to solve for pure substances, though it gives very accurate results in the gaseous region compared to measurement data. The equation of state (EOS) is given by

$$p = \frac{RT}{v-b} - \frac{a(T)}{v^2 + 2 \cdot bv - b^2} \tag{15}$$

where $a(T)$ and b represent attractive or repulsive molecular forces, respectively. Both parameters can be obtained by pressure p_c and temperature T_c at the critical point:

$$a(T) = 0.45724 \frac{R^2 T_c^2}{p_c} \cdot \left[1 + \kappa\left(1 - T_r^{1/2}\right)\right]^2, \qquad b = 0.07780 \frac{RT_c}{p_c}. \tag{16}$$

Here, κ is an empirical, substance-specific parameter given by $\kappa = 0.37464 + 1.54226\omega - 0.26992\omega^2$ and ω is the acentric factor presented in [16], which indicates the deviation of the fluid's molecule shape from an ideal sphere. For carbon dioxide and the natural gas mixture, we can determine the acentric factor to $\omega_{\text{CO}_2} = 0.2249$ and $\omega_{\text{NG}} = 0.032$, where ω_{NG} has been averaged over both components, nitrogen and methane, according to the respective mole fractions. To determine the compressibility factor Z, we can rewrite (15) according to [15] and get the following cubic equation:

$$Z^3 - (1-B)Z^2 + (A - 2B - 3B^2)Z - B(A - B - B^2) = 0 \tag{17}$$

with

$$A = \frac{ap}{R^2 T^2}, \qquad B = \frac{bp}{RT} \tag{18}$$

which can be solved easily using *Cardano*'s method. To obtain the compressibility factor of the binary mixture, we use the following mixing rule to average Z according to the mass fraction x of each component i:

$$Z_{\text{mix}} = \sum_i x_i Z_i. \tag{19}$$

The mixture's thermodynamic and transport properties are determined in the same way. Viscosity μ, thermal conductivity λ, and heat capacity c_p are functions of density or pressure and temperature, valid for pure substances. We use equations similar to (19) to obtain the respective properties for the mixture.

3. Benchmarking

To verify the numerical compressible flow model, we perform a simulation in a simplified model geometry and compare the results with an analytical solution presented by Häfner et al. [17]. We consider a 1D, axisymmetric model domain with a gas injection well in the center (see Fig. 2). At this well ($r = r_0 = 0.1$ m), we consider a constant injection pressure $p(r_0, t) = p_0$. The outer radius R denotes the boundary of the reservoir at a distance to the center of $R = 1$ km. This boundary is closed, i.e. there is no gas flow across it ($\partial p/\partial r = 0$). The domain consists of a homogeneous material with a permeability of $k = 1 \cdot 10^{-14}$ m^2 and a porosity of $n = 0.1$.

In order to obtain an analytical solution, we have to linearize the problem by considering both Laplace and mass balance coefficients in (8) to be constant. Fig. 3 shows that both coefficients $D = \frac{k\rho}{\eta Z}$ and $S = \frac{n\beta_f p}{Z}$ are strongly depending from pressure when we are assuming real gas behavior. With growing pressures, the variability of fluid properties is decreasing. Thus, we choose a very high initial reservoir pressure of $p_i = 35$ MPa and an injection pressure of $p_0 = 40$ MPa at isothermal temperature of $T = 330$ K. At these conditions, D and S can considered to be constant since the slope of both curves is moderate.

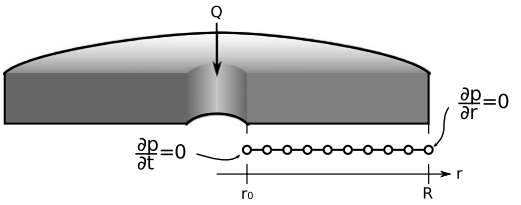

Fig. 2. Schematic of the axisymmetric reservoir for benchmarking purposes and 1D-FEM representation of the domain accounting for radial symmetry. Reservoir boundaries at $r = R$ are closed ($\partial p/\partial r = 0$) and a constant pressure ($\partial p/\partial t = 0$) is applied at the borehole boundary $r = r_0$.

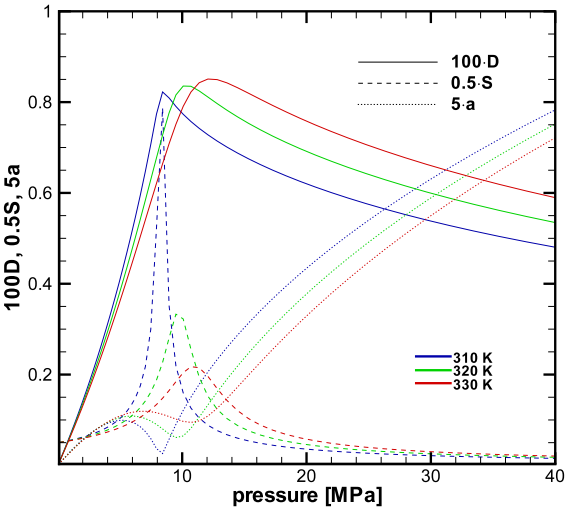

Fig. 3. Coefficients $D = \frac{k\rho}{\eta Z}$ and $S = \frac{n\beta_f p}{Z}$ as well as $a = \frac{D}{S}$ of Eq. (8) versus pressure at 310, 320, and 330 K isotherm.

The working fluid in this example is pure CO_2, and we used the equation of state (15) for the determination of fluid compressibility $\beta_f(35\ \text{MPa}, 330\ \text{K}) = 0.079$ and of compressibility factor $Z(35\ \text{MPa}, 330\ \text{K}) = 0.63$. Viscosity has been derived by the correlation of Fenghour [18] which outcomes to $\mu = 8.9 \cdot 10^{-5}$ Pa s. We performed a numerical simulation using constant coefficients D and S to compare the results of simulation and exact solution. The discretization of the model annulus has been done using 1D line elements, consisting of two nodes each. The length of every element increases with growing distance from the center, and lies between 0.01 m at the injection well and 10 m at the outer border.

The comparison of numerical and analytical solutions of the benchmark problem is shown in Fig. 4. Both solutions show a perfect agreement for the linearized problem, so we can consider our model to be valid. It was assumed, that the variability of coefficients D and S at the pressure range 35 MPa $\leq p \leq$ 40 MPa is low enough to consider the problem to be linear. Fig. 5 shows the comparison of both linearized and non-linear numerical solution under this condition. The deviation between both results is very small, since the fluid properties are almost constant at these high pressures. At lower pressures, as shown in Fig. 6, this assumption cannot be made. Fluid properties of gases show a non-linear behavior. So, the solution of (8) can only be found using numerical methods when realistic behavior of fluids is to be considered.

4. EGR Application

4.1. The Altmark gas field

Due to natural gas production since the nineteen-twenties, the former reservoir pressure level of the *Altmark* gas field has been reduced to about 30–40 bar. The temperature in the reservoir has been equilibrated to approximately 125 °C. Various layers of halite and cap rock act as natural barriers and assure the reservoir's sealing. The main components of the residing gas in the field are nitrogen (≈75%), methane (≈25%), and a residual amount of carbon dioxide. Other components such as ethane, propane, helium, and water appear only in traces and are neglected in this work.

4.2. Material properties

Gas flow in porous media strongly depends on both solid and fluid material properties. Fluid properties can be determined by many well-known theories and correlations: for viscosity, we used the correlations of Fenghour [18] for CO_2, Stephan [19]

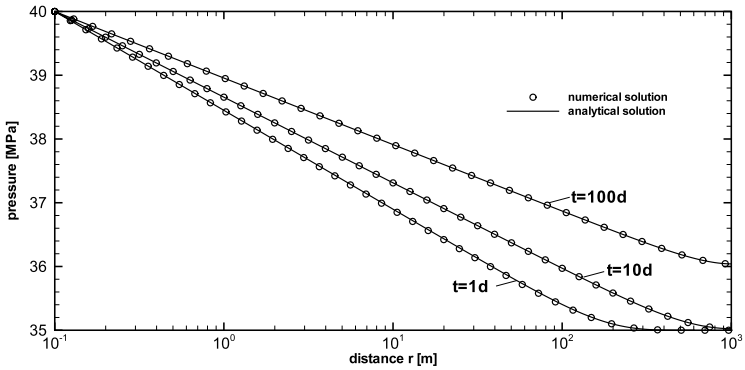

Fig. 4. Comparison of analytical and numerical solution for constant parameters $D(p_i)$ and $S(p_i)$. Borehole pressure was set to $p_b = 40.0$ MPa, initial reservoir pressure was $p_i = 35.0$ MPa. Isothermal temperature was set to $T = 330$ K. Both solutions show a perfect agreement.

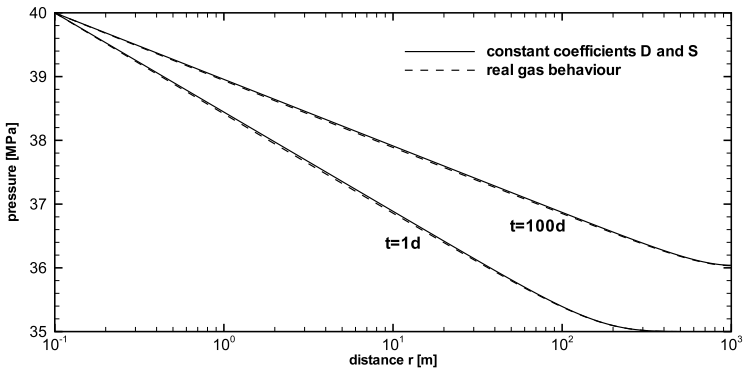

Fig. 5. Comparison of linearized and non-linear problem at the same pressure range as shown in Fig. 4. At this condition, fluid properties are almost constant, so the differences between linear and non-linear assumption is very small.

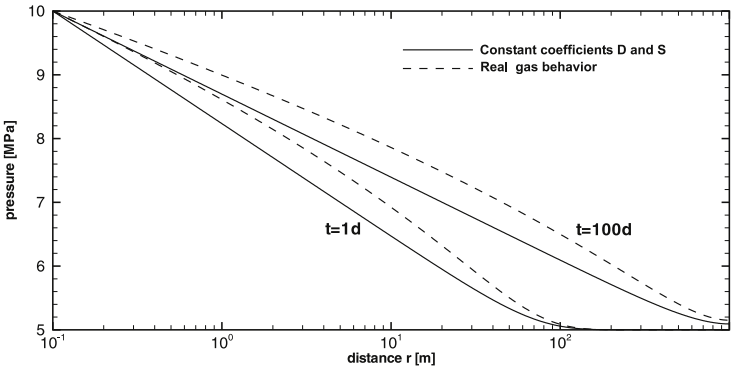

Fig. 6. Comparison of linearized and non-linear problem at pressures around the critical region. In this condition range, fluid properties cannot considered to be constant, the difference between linear and realistic assumption is remarkable.

for N_2 and Friend [20] for CH_4. In the same way, we used Vesovic [21], Stephan [19], and Younglove [22] for the determination of thermal conductivity. Heat capacities of fluids have been derived from the fundamental equation of thermodynamics in [23–25]. Although these relations are functions of fluid density and temperature, we used constant values for the heat capacities of the fluids to minimize the computational effort. This simplification can be made since both, injected and residing fluids, are gases. So, the difference of the heat capacities at reservoir and injection conditions can be neglected. For higher pressures, e.g., at liquid or supercritical conditions, heat capacity differences may have a much higher influence.

All fluid properties are determined for pure substances and averaged for the mixture according to each fluid's mass fraction. The coefficient of molecular diffusion, D_m, has been determined according to the *Chapman–Enskog* theory taken from Cussler [26]. According to collision diameters and intermolecular potential parameters found in [27], we determined the diffusion coefficient to be $D_m = 1.213 \cdot 10^{-5}$ m^2 s^{-1} at $T = 300$ K and $p = 4$ MPa. The ranges of all fluid properties are shown in Table 1.

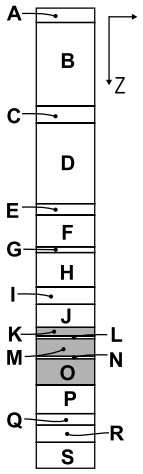

	dh [m]	K [m²]	n [-]	c_p^s [J/kg/K]	λ^s [W/m/K]	ρ^s [kg/m³]
A	5	$2\cdot10^{-16}$	0.039	1300	2.6	2460
B	29	$3\cdot10^{-19}$	0.01	1200	2.1	2940
C	6	$5\cdot10^{-16}$	0.046	1000	2.1	2940
D	28	$5\cdot10^{-19}$	0.011	1200	2.1	2700
E	4	$2\cdot10^{-15}$	0.021	1000	2.6	2940
F	11	$5\cdot10^{-19}$	0.011	1200	2.1	2700
G	2	$2\cdot10^{-17}$	0.025	1300	2.7	2940
H	12	$5\cdot10^{-19}$	0.011	1200	2.1	2700
I	6	$5\cdot10^{-15}$	0.073	1100	2.3	2940
J	8	$5\cdot10^{-19}$	0.011	1200	2.1	2700
K	3	$2\cdot10^{-13}$	0.162	1500	3	2940
L	1	$5\cdot10^{-19}$	0.011	1200	2.1	2700
M	6	$2\cdot10^{-13}$	0.154	1000	2.1	2940
N	1	$5\cdot10^{-19}$	0.011	1200	2.1	2700
O	9	$3\cdot10^{-13}$	0.172	1400	2.7	2940
P	10	$5\cdot10^{-19}$	0.011	1200	2.1	2700
Q	4	$8\cdot10^{-15}$	0.082	1300	2.7	2940
R	6	$5\cdot10^{-19}$	0.011	1200	2.1	2720
S	9	$2\cdot10^{-17}$	0.023	1200	2.2	2940

Fig. 7. Layered structure of the near-well reservoir. In the table, *dh* indicates horizon thicknesses, **K** is permeability, *n* is porosity, c_p^s, λ^s, and ρ^s are heat capacity, thermal conductivity and density of the solid material. The gray highlighted layers K, M, and O are the most permeable horizons.

Table 1
Fluid properties of pure CO_2 and pure natural gas (NG) at undisturbed reservoir conditions ($p = 3.5$ MPa, $T = 400$ K) and at injection conditions ($p = 4.3$ MPa, $T = 300$ K).

Fluid	Density (kg/m³)	Viscosity (Pa s)	Thermal conductivity (W/m/K)
Reservoir conditions			
CO_2	49.86	$2.01 \cdot 10^{-5}$	0.0333
NG	26.29	$2.06 \cdot 10^{-5}$	0.0381
Injection conditions			
CO_2	104.02	$1.62 \cdot 10^{-5}$	0.023
NG	44.23	$1.70 \cdot 10^{-5}$	0.031

The properties of the porous medium have been selected based on investigations of Pusch [28]. The target area of the reservoir consists of 19 discriminable material layers (see Fig. 7). Layers B, D, F, H, J, L, N, P, and R can be considered to be natural barriers, since their permeability is less than 1 μD (1D $= 9.86923 \cdot 10^{-13}$ m^2). Layers A, C, E, G, I, Q, and S do not play an important role for the storage process either, their permeabilities are less then 5 mD and their porosities are between 1% and 8%. The interesting layers for storage and transport processes are layers K, M, and O. These layers consist of high permeabilities (170–300 mD), large porosities (15–17%) and adequate thicknesses (3, 6, and 9 m).

The hydrodynamic dispersivity α of a porous medium is an empirical factor which represents the smoothing of concentration gradients. According to Gelhar [29], the longitudinal dispersivity α_L shows a clear trend of systematic increase with the scale of the problem. But, the degree of uncertainty of dispersivity is very high. Several approximations to obtain a value for α_L have been presented [30–32]. We choose two of them, introduced in [30]. Both correlations are regressions based on the same dataset, but using different weighting schemes:

$$\alpha_{L,1} = 1.2\,(\log_{10} L)^{2.958} \qquad \alpha_{L,2} = 0.83\,(\log_{10} L)^{2.414}\,. \tag{20}$$

We chose the characteristic length L to be our model domain radius, so $L = 10\,000$ m and obtain $\alpha_{L,1} = 72.4$ m and $\alpha_{L,2} = 23.6$ m. In general, it is accepted to estimate the transversal dispersivity α_T to be one magnitude lower than the longitudinal dispersivity. Thus, we choose transversal dispersivities to be $\alpha_{T,1} = 7.2$ m or $\alpha_{T,2} = 2.4$ m, respectively.

4.3. Numerical simulation

Software. We use the open-source scientific software OpenGeoSys (OGS, Wang [33]) for our simulations. OGS is a numerical tool for modeling coupled thermo, hydro, mechanical and chemical (THMC) processes in porous or fractured media using an object-oriented finite element method. A large number of benchmark tests and applications have been performed to verify the validity of this simulation tool [14,11,10,12,34].

Discretization. The study area has a layered shape consisting of 19 different material groups. Since we are considering the near-well region of the reservoir, we neglect heterogeneities in horizontal direction. Thus, we designed our model domain as a 2D vertical plane, which is axisymmetric around the injection well. The outer boundary should not be affected by the injection process, so we chose its location far away (at a distance of $r = 10\,000$ m) from the well. The plane consists of 103 elements with increasing length in r direction and 3 elements for each material layer in z direction, which yields to

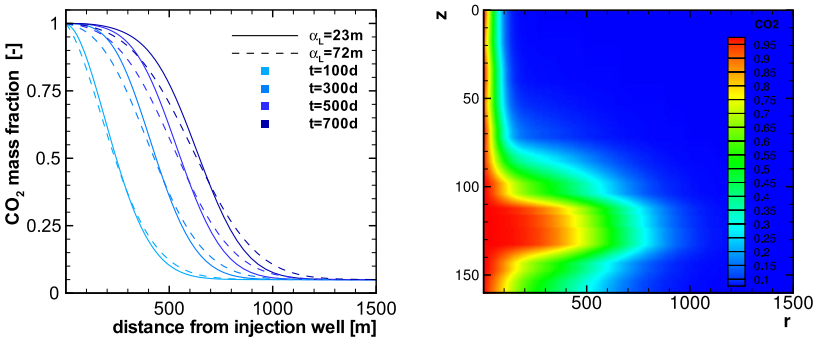

Fig. 8. CO_2 distribution within *O* horizon at four times and two different dispersivities (a). 2D-plot of CO_2 distribution within the reservoir for $r \leq 1500$ m when dispersivity is $\alpha_L = 72.4$ m(b).

5871 rectangular elements. We performed a non-isothermal simulation of the EGR process over a period of 2 years. At the beginning of the injection process, when pressure, temperature, and concentration gradients are very large, the temporal discretization was chosen to be small ($dt = 1$ s). With growing simulation time, the interface moves away from the injection well, so the flow velocity is decreasing (due to axisymmetry). Smaller velocities allow the timestep size to increase, so we could end up with a timestep length of 100 d. Non-isothermal effects, such as *Joule–Thomson* effect or viscous heat dissipation have been neglected in our study; those effects have been investigated in [35] for comparable situations. From this work, we can assume that the heat loss due to gas expansion would only affect the direct vicinity of the injection well, and the temperature difference would be low (less than 1 K at comparable conditions). However, these effects could be very important at supercritical pressures or for conditions close to the phase boundaries, which is not the case at the current conditions in this study.

Initial and boundary conditions. Initially, our model reservoir is filled with a mixture of natural gas (consisting of 75% N_2 and 25% CH_4) and a residual concentration of CO_2. The CO_2 mass fraction is $x_{CO_2} = 0.05$ before the injection starts. The initial reservoir pressure is $p_0 = 35$ MPa, distributed following the hydrostatic gradient according to the mixture density, which is $\rho_{\text{mix}} \approx 28$ kg/m^3. The reservoir temperature is $T_0 = 400$ K, distributed uniformly. The simulated CO_2 injection takes place at uniform injection pressure $\partial p/\partial t = 0$ and temperature $\partial T/\partial t = 0$ at the injection well located in the center of the 2D axisymmetric plane. The injection pressure is $p_i = 4.3$ MPa which has been estimated by static calculations to result in a total mass flux of approximately 50 000 metric tons of CO_2 per year. The outside boundary of the reservoir at $r = 10\,000$ m is impermeable, so $\partial p/\partial r = 0$.

Results. Fig. 8(a) shows the CO_2 mass fraction in the reservoir *O* horizon, located at 122 m $\leq z \leq$ 131 m after 100, 300, 500, and 700 days of continuous injection. The solid lines represent the results obtained when dispersivity $\alpha_L = 23.6$ m, while the dashed lines show results for $\alpha_L = 72.4$ m. This horizon shows the fastest CO_2 transport velocity. For comparison, the expansion of the gas in the other horizons can be seen in Fig. 8(b).

When injecting CO_2 into a depleted, closed gas reservoir, the pressure will increase slowly up to its former, undisturbed level. Since our goal was to consider only the near-well region of the gas field, we expanded the model domain so that the outer boundary is not affected by the pressure increase (see Fig. 9(a)). Thus, we can consider the heat and mass transport processes in the vicinity of the injection well as if the reservoir would be infinite.

Comparing Figs. 8(a) and 9(b), we can see that the expansion of heat is much slower than the expansion of CO_2. The reason of this difference is the large heat storage capacity of the solid rock material. The cooling down effect has expanded up to a distance of $r \approx 100$ m after 2 years of injection, while the CO_2 plume has reached a distance of $r \approx 1000$ m. This explains the steplike shape of the fluid property correlation plots shown in Fig. 9(c) for density and Fig. 9(d) for viscosity. The high density (and low viscosity) region at 0.5 m $\leq r <$ 100 m results from the low temperatures in that region. Between 100 m $< r <$ 1000 m, we see the properties of a CO_2-*natural gas* mixture and at $r >$ 1000 m, the curves represent the properties of pure *natural gas*. To monitor the fluid and reservoir conditions across all horizons, we insert a virtual observation well at $r = 10$ m. Fig. 10 shows pressure and temperature conditions as well as density and viscosity of the fluid mixture versus the thickness of the reservoir. Every second horizon in this figure is colored gray to distinguish between individual reservoir layers. The total mass of injected CO_2 can be determined by

$$m_{CO_2} = 2\pi\rho \int_{t_0}^{t_1} \sum_i \Delta z_i v_{r,i} dt \tag{21}$$

where i is the horizon number, z_i are the thicknesses of the different material horizons, and $v_{r,i}$ is the velocity of CO_2 in r direction, averaged over each horizon thickness. From (21), we obtain the total mass of CO_2 injected into the gas field over the period between $t_0 = 0$ a and $t_1 = 2$ a to be $m_{CO_2} = 110\,600$ t, which lies within the expected range. 98% of that mass is distributed in horizons *K*, *M*, and *O*.

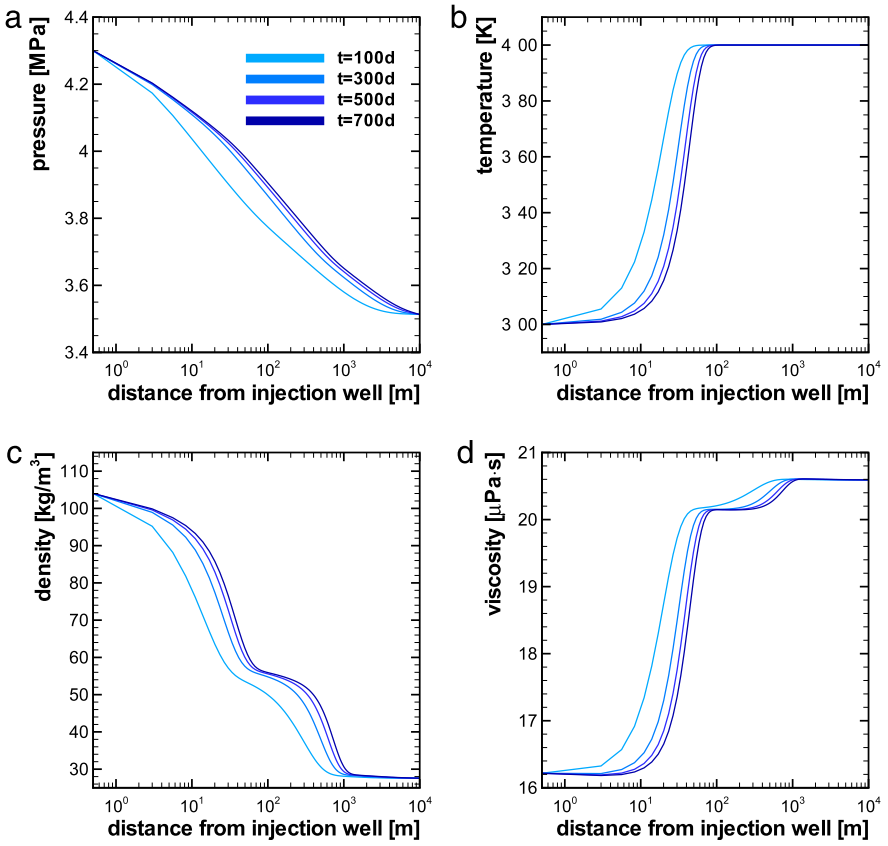

Fig. 9. Pressure (a), temperature (b), density (c), and viscosity (d) along *O* horizon.

5. Summary and outlook

In this work, we developed a numerical model for non-isothermal fluid flow in porous media. Thereby, compressibility of fluids according to semi-empirical equations of state have been taken into account. It was important to use an approach which allows the EOS to be chosen freely depending on the working fluid and on the specific needs of the problem. The numerical modeling tool has been implemented into the open-source simulator OpenGeoSys and can be used for various kinds of applications such as carbon dioxide capture and storage, natural gas storage or geothermal energy generation.

By comparing the model results to a simplified analytical solution, the model output could be verified for isothermal real gas flow problems. The performed benchmark shows the applicability of the model tool for gas storage applications and the necessity of numerical solving techniques for non-linear flow. To show the capabilities of the model tool, we performed a simulation of an enhanced gas recovery application at a specific site. We could investigate the distance of CO_2 expansion in the reservoir when 100 000 tons of CO_2 are injected into the *Altmark* field over a period of two years. This simulation illustrated important consequences of the injection, such as the temporal development of pressure increase or the reservoir cooling down due to the cold working fluid. However, our simulations did not cover the whole EGR process, we performed only an example simulation based on realistic data on the field scale. The simulations described in Section 4 correspond only to the near-well region and neglect the influences of a production well.

For the design of an EGR application, many questions have to be taken into account. To answer these questions, the shape of our model domain could be redesigned for a field scale, 3D simulation and one or more production wells could be included. The model output will be helpful to answer questions concerning ecological benefits (e.g. amount of storable CO_2), economical feasibility (e.g. amount and pureness of produced natural gas), safety (e.g. pressure and temperature development over time), or timescales (e.g. time until the former natural pressure level is reached). Getting answers to these questions is necessary for the planning of new EGR applications and the estimation of possible risks.

Acknowledgments

This work has been funded by the German Federal Ministry of Education and Research (BMBF). The authors acknowledge the cooperation with GDF SUEZ E&P Deutschland GmbH and appreciate the supply of field data.

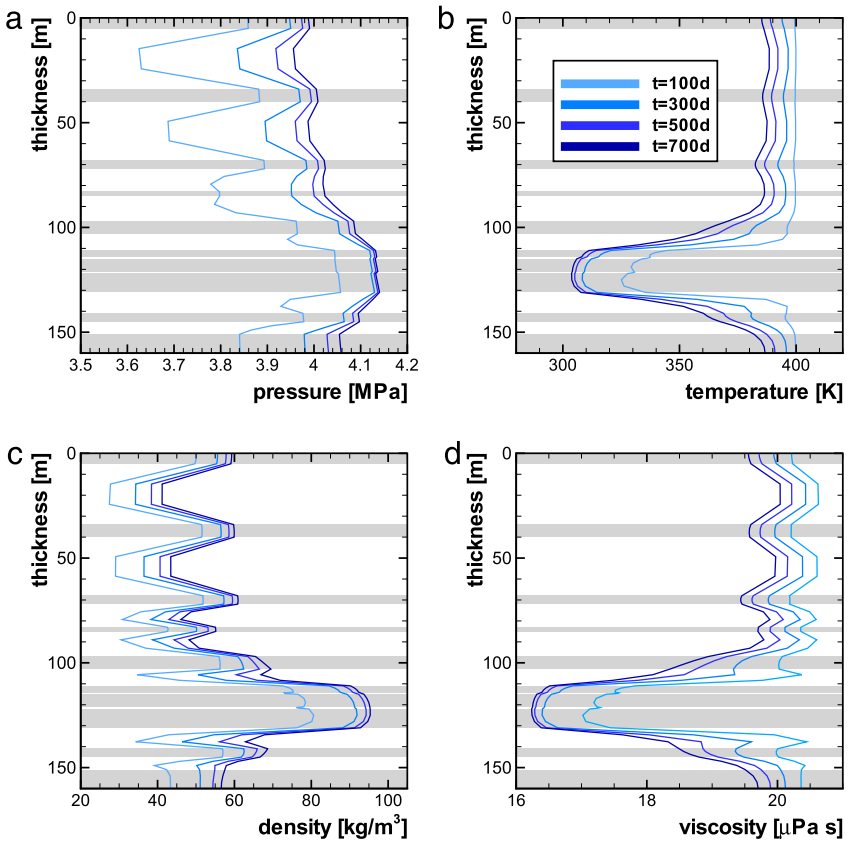

Fig. 10. Pressure (a), temperature (b), density (c), and viscosity (d) versus reservoir depths at an observation well at $r = 10$ m. The different material layers are indicated by white/ gray bars.

References

[1] International Energy Agency, World Energy Outlook, 2010.
[2] The CO_2-MOPA project. Webpage: http://www.co2-mopa.de/.
[3] The CO_2-SINK project. Webpage: http://www.co2sink.org/.
[4] K. Blok, R.H. Williams, R.E. Katofsky, C.A. Hendricks, Hydrogen production from natural gas, sequestration of recovered CO_2 in depleted gas wells and enhanced gas recovery, Energy 22 (1997) 161–168.
[5] C.M. Oldenburg, S.H. Stevens, S.M. Benson, Economic feasibility of carbon sequestration with enhanced gas recovery (CSEGR), Energy 29 (2004) 1413–1422.
[6] M.J. van der Burgt, J. Cantle, V.K. Boutkan, Carbon dioxide disposal from coal based IGCC's in depleted gas fields, Energy Convers. Manage. 33 (1992) 603–610.
[7] S. Holloway, Underground sequestration of carbon dioxide-a viable greenhouse gas mitigation option, Energy 30 (2005) 2318–2333.
[8] The CLEAN project. Webpage: http://www.clean-altmark.org/.
[9] M. Kühn, A. Förster, J. Großmann, R. Meyer, K. Reinicke, D. Schäfer, H. Wendel, CLEAN: preparing for a CO_2-based enhanced gas recovery in a depleted gas field in Germany, Energy Procedia 4 (2011) 5520–5526.
[10] C.-H. Park, J. Taron, U.-J. Görke, A.K. Singh, O. Kolditz, The fluidal interface is where the action is in CO_2 sequestration and storage: hydromechanical analysis of mechanical failure, Energy Procedia 4 (2011) 3691–3698.
[11] U.-J. Görke, C.-H. Park, W. Wang, A.K. Singh, O. Kolditz, Numerical simulation of multiphase hydromechanical processes induced by CO_2 injection in deep saline aquifers, Oil Gas Sci. Technol. 66 (1) (2011) 105–118.
[12] B.J. Graupner, D. Li, S. Bauer, The coupled simulator ECLIPSE-OpenGeoSys for the simulation of CO_2 storage in saline formations, Energy Procedia 4 (2011) 3794–3800.
[13] J. Bear, Dynamics of Fluids in Porous Media, American Elsevier, 1972.
[14] A.K. Singh, N. Böttcher, W. Wang, C.-H. Park, U.J. Görke, O. Kolditz, Non-isothermal effects on two-phase flow in porous medium: CO_2 disposal into a saline aquifer, Energy Procedia 4 (2011) 3889–3895.
[15] D.Y. Peng, D.B. Robinson, A new two-constant equation of state, Ind. Eng. Chem. Fundam. 15 (1974) 59–64.
[16] K.S. Pitzer, Corresponding states for perfect liquids, J. Chem. Phys. 7 (8) (1939) 583–590.
[17] F. Häfner, D. Sames, H.-D. Voigt, Wärme-und Stofftransport-Mathematische Methoden, Springer-Lehrbuch, 1992.
[18] A. Fenghour, W.A. Wakeham, V. Vesovic, The viscosity of carbon dioxide, J. Phys. Chem. Ref. Data 27 (1998) 31–44.
[19] K. Stephan, R. Kraus, A. Laesecke, The viscosity and thermal conductivity of nitrogen for a wide range of fluid states, J. Phys. Chem. Ref. Data 16 (4) (1987) 993–1023.
[20] D.G. Friend, J.F. Ely, H.H. Ingham, Thermophysical properties of methane, J. Phys. Chem. Ref. Data 18 (2) (1989) 583–638.
[21] V. Vesovic, W.A. Wakeham, The transport properties of carbon dioxide, J. Phys. Chem. Ref. Data 19 (3) (1990) 763–807.
[22] B.A. Younglove, J.F. Ely, Thermophysical properties of fluids. II. methane, ethane, propane, isobutane and normal butane, J. Phys. Chem. Ref. Data 16 (4) (1989) 577–798.
[23] R. Span, W. Wagner, A new equation of state for carbon dioxide covering the fluid region from the tripple point temperatur to 1100 K and at pressures up to 800 MPa, J. Phys. Chem. Ref. Data 25 (6) (1996) 1509–1596.

[24] U. Setzmann, W. Wagner, A new equation of state and tables of thermodynamic properties for methane covering the range from the melting line to 625 K at pressures up to 1000 MPa, J. Phys. Chem. Ref. Data 20 (6) (1991) 1061–1155.
[25] R. Span, E.W. Lemmon, R.T. Jacobsen, W. Wagner, A. Yokozeki, A reference equation of state for the thermodynamic properties of nitrogen for temperatures from 63.151 to 1000 K and pressures to 2200 MPa, J. Phys. Chem. Ref. Data 29 (2000) 1361–1431.
[26] E.L. Cussler, Diffusion-Mass Transfer in Fluid Systems, Cambridge University Press, Cambridge, New York, 1997.
[27] J. Hirschfelder, C.F. Curtiss, R.B. Bird, Molecular Theory of Gases and Liquids, Wiley, New York, 1954.
[28] G. Pusch, G.F. Ionescu, F May, G. Voigtländer, L. Stecken, D. Vosteen, Common features of carbon dioxide and underground gas storage, Oil Gas European Magazine 36 (3) (2010) 131–136.
[29] L.W. Gelhar, C. Welty, K.R. Rehfeldt, A critical review of data on field-scale dispersion in aquifers, Water Resour. Res. 28 (7) (1992) 1955–1974.
[30] M. Xu, Y. Eckstein, Use of weighted least-squares method in evaluation of the relationship between dispersivity and field scale, Ground Water 33 (6) (1995) 905–908.
[31] S.P. Neuman, Universal scaling of hydraulic conductivities and dispersivities in geologic media, Water Resour. Res. 26 (8) (1990) 1749–1758.
[32] A. Ayra, Dispersion and reservoir heterogeneity, Ph.D. Dissertation, University of Texas, Austin, TX, 1986.
[33] W. Wang, J. Rutqvist, U.J. Görke, J.T. Birkholzer, O. Kolditz, Non-isothermal flow in low permeable porous media: a comparison of Richards' and two-phase flow approaches, Environ. Earth. Sci. 62 (2011) 1197–1207.
[34] D. Li, B. Graupner, S. Bauer, A method for calculating the liquid density for the CO_2–H_2O–NaCl system under CO_2 storage condition, Energy Procedia 4 (2011) 3817–3824.
[35] A.K. Singh, U.J. Görke, O. Kolditz, Numerical simulation of non-isothermal compositional gas flow: application to carbon dioxide injection into gas reservoirs, Energy 36 (2011) 3446–3458.